Journal of Magnetic Resonance 207 (2010) 53–58

Contents lists available at ScienceDirect

Journal of Magnetic Resonance

journal homepage: www.elsevier.com/locate/jmr

Determining object boundaries from MR images with sub-pixel resolution: Towards in-line inspection with a mobile tomograph

Ernesto Danieli [a], Klaus Berdel [b], Juan Perlo [a], Walter Michaeli [b], Ullrich Masberg [b], Bernhard Blümich [a], Federico Casanova [a,*]

[a] Institut für Technische Chemie und Makromolekulare Chemie, RWTH Aachen University, Worringerweg 1, D-52074 Aachen, Germany
[b] Institute of Plastics Processing at RWTH Aachen University, Pontstrasse 49, D-52062 Aachen, Germany

ARTICLE INFO

Article history:
Received 29 April 2010
Revised 6 August 2010
Available online 14 August 2010

Keywords:
Mobile MRI
Halbach arrays
Permanent magnets
Edge-detection
In-line inspection
Extrusion process

ABSTRACT

This work evaluates the performance of edge-detection algorithms to determine the sample geometry with high spatial accuracy from low-resolution MR images. In particular, we show that by applying such numerical methods it is possible to reconstruct the internal and external contours of the object with a spatial precision that surpasses the nominal spatial resolution of the image by more than one order of magnitude. Special attention is paid to find the spatial resolution and signal-to-noise ratio required by the described numerical methodology to achieve a desired spatial accuracy. Finally, we discuss the potential application of this image processing approach for in-line quality control of extruded rubber materials, where micrometer spatial precision has to be achieved from images measured in short experimental times. The results presented here prove that the sensitivity of mobile MRI sensors is enough to achieve the spatial accuracy required to proof check the production of extruded rubber fittings in acceptable experimental times.

1. Introduction

Magnetic resonance imaging (MRI) is a powerful non-invasive technique routinely used for medical diagnostics. Compared to X-ray or ultrasound tomography, MRI offers an outstanding diversity of contrast in soft matter that can be applied to resolve tissues of similar density but different molecular structure, morphology, and even molecular mobility. The possibility to spatially resolve physical and chemical properties across the sample under study has spread the application of MRI into several areas of material science [1,2]. Although several industrial processes would considerably benefit from the implementation of MRI at the production site, the required equipment typically cannot be installed in a production area for technical and security reasons. Conventional MRI magnets use expensive and sophisticated superconducting coils to generate strong and homogeneous magnetic fields. In general they are bulky units that require large footprint to assure sufficient distance to personnel and the magnetic material in the surrounding. Moreover, the fragility of the superconducting wires cooled to liquid helium temperature limits the mobility of the tomograph and its use at different stages of a production line. Finally, the operation of the magnet requires permanent maintenance with cryogenic coolants which further complicates the use of such magnets on the factory floor.

Most of these limitations can be overcome by discarding superconducting magnets in favor of portable magnet arrays built from permanent magnetic materials instead of superconducting coils. These magnets have been largely avoided in the past due to their poor performance in terms of field strength and homogeneity, but thanks to a novel shimming strategy, the large magnetic field inhomogeneities inherent to permanent magnetic materials can be efficiently corrected [3]. This shimming concept uses a set of movable magnets included in the magnet array by which spherical harmonic correction terms to the magnetic field can be generated. After mapping the magnetic field in the volume of interest, the inhomogeneities are decomposed in the basis set of the movable magnets and the required displacement of the shim blocks are calculated. An iterative application of this procedure leads to homogeneity improvements up to values very close to the optimal performance predicted by numerical simulations with ideal magnet blocks. By applying this approach we have recently demonstrated that mobile magnets can be used to measure magnetic resonance images free of distortions caused by background gradients [4,5].

Although achieving these experimental conditions with portable magnets opens the door to implementing MRI at the production site, at the time of considering these setups for in-line control, the fact that the total time available for the measurement

* Corresponding author. Fax: +49 241 8022185.
E-mail address: fcasanova@mc.rwth-aachen.de (F. Casanova).

1090-7807/$ - see front matter © 2010 Elsevier Inc. All rights reserved.
doi:10.1016/j.jmr.2010.08.004

is limited, considerably affects the quality of the images [6,7]. This problem is particularly severe for samples with short relaxation times T_2, where slow imaging methods sampling the k-space line-by-line must be used. Under these conditions it becomes very challenging to achieve a nominal spatial resolution comparable to object size deviations tolerated by quality standards. At this point, the use of edge-detection algorithms developed in the imaging processing area appears to be the solution to reconstruct the geometry of the sample with an accuracy better than the nominal resolution [8–10]. In this work we investigate the performance of such algorithms to determine the geometrical structure of the samples with high spatial accuracy from images measured with modest spatial resolution in a mobile MRI system. In particular, we show that from images with a nominal spatial resolution of 1 mm^2 this methodology can extract the cross section of the sample with an accuracy of some tens of a micrometer. Since the achievable sub-pixel resolution is determined by the signal-to-noise ratio in the image, for these we used studies a tomograph based on a recently optimized compact magnet geometry [5]. It generates about the highest field strength achievable with a magnet of such dimensions, maximizing the sensitivity of the sensor.

Besides setting the limits and conditions required for the implementation of sub-pixel algorithms, the experimental results presented in this work demonstrate that mobile MRI is at the stage to be used for quality control in-line at real time. The described methodology is applied to MR images of extruded polymer materials. Rubber fittings, for example, are produced by continuous extrusion of uncured rubber through a die that defines its shape. In general, multiple rubber mixtures are co-extruded and vulcanized to meet specific properties and mechanical stability, making such fittings suitable for their use in the building and automotive industry. Knowledge about the material properties, surface quality, and profile dimensions, is essential for quality control [11–14]. Depending on the type of contrast, MRI images could provide information about filler distribution, specific gravity, shore hardness, and cross-link density, which nowadays are typically tested off-line by random sampling and manual inspection [12,14]. We demonstrate that for this type of industrial process, edge-detection algorithms can be applied to obtain the inner and outer contours of such profiles with the required spatial accuracy from images measured with a mobile MRI system. It is important to notice that even though optical methods have become commercially available for in-line quality control, they are limited to monitor only the external dimensions of the profile (optical methods are used to inspect the inner shape off-line after profiles are cut [15]).

2. Rubber extrusion

Fig. 1a shows a scheme of a rubber extrusion line used to continuously produce rubber fittings. In the extrusion process, uncured rubber is continuously transported by a screw rotation in a cylinder from a feed port to the die of the extruder. At the extrusion die, the profile is formed out to its final shape. Usually, it is also possible to find a co-extrusion process where multiple layers or parts of different material are simultaneously extruded. By applying this technique, or by integrating inlays made of other materials, e.g. thermoplastic polymers, textiles or metals, the physical properties of the rubber profile can be tailored to meet the technical demands. After its shaping, the profiles are vulcanized in the curing unit of the extrusion line. Here, the material develops elastic properties and becomes geometrically stable. Further processing steps, e.g. flocking, can be applied and the profiles are packaged. The length of typical extrusion lines exceeds 100 m.

Since rubber is a viscoelastic material, when it leaves the extrusion die effects like swelling, draw down, cooling and relaxation start affecting the actual size and shape of the extrudate. These effects are not stationary and non-linear. Especially for rubber mixtures, with up to more than 30 ingredients, they are still not yet fully understood [11,12,16]. Thus, the geometry of an extruded profile is not only depending on the shape of the extrusion die. It is influenced by several interdependent process parameters, such as the temperature distribution in the extruder, its screw speed, the take-off speed of the extrusion line, the viscosity of the samples, etc. Therefore, starting-up an extrusion process for a new product requires adjustments of the mentioned variables. This is a time consuming procedure that requires feedback quantifying the product geometry and leads to many meters of start-up scrap inhibiting a wrong geometry, which are produced while the user adapts the process parameters [11]. Moreover, once the parameters are adjusted, in a running extrusion process disturbances due to several reasons are likely to occur [12] leading to a lower

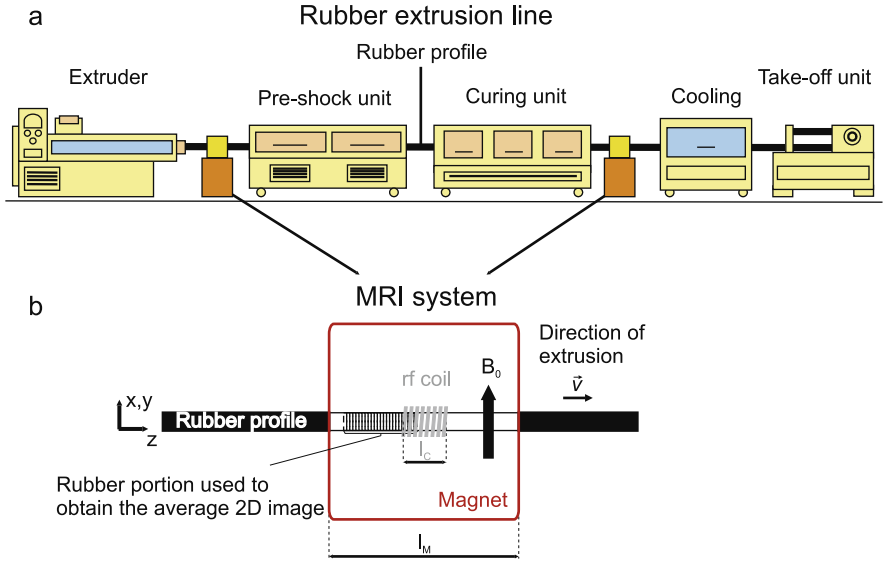

Fig. 1. (a) General scheme of an extrusion line showing the potential places where the MRI monitoring system could be mounted. (b) Scheme of the MRI system where the extrusion direction z and the transverse xy-plane are shown. By using a Halbach magnet, the direction of the magnetic field, transverse to the magnet axis, allows the use of a solenoid rf coil which is also schematized.

product quality. For example, even an open door in the extrusion shop in winter can lead to a local cooling of the extrusion line, disturbing the curing of the rubber and thus influencing the geometry of the profile over a considerable length on the profile. In the next sections we discuss the possibility to obtain detailed and early knowledge of the inner geometry and the distribution of different material flows by placing in the extrusion line a mobile MRI sensor as shown in Fig. 1.

3. Results and discussion

A mobile MRI sensor as the one described in Section 4 was used to measure cross-sections of rubber seals produced for automotive applications. Since the relaxation time values, $T_1 = 20$ ms and $T_2 = 2.7$ ms, of these samples measured at room temperature are relatively short, the MRI methodology implemented was a spin-echo sequence with the shortest echo time possible [1,2]. It should be noted that due to the short T_2 of the studied rubber samples, only very short acquisition times could be used. For this reason the high homogeneity of the magnet is not exploited for the present studies, and images with the same sensitivity could be obtained with magnets generating the same field strength and just modest homogeneity. Field inhomogeneity can be tolerated as soon as the background gradients do not distort the images.

Fig. 2a shows a 2D MR image of a slice of the rubber seal measured at rest using this sequence. It consists of 64×64 pixels with a slice thickness of 10 mm excited using selective 90° and 180° Sinc2 pulses with a length of 100 μs. The spin-echo was sampled during 640 μs, which determines an echo time $T_E = 800$ μs. The image was obtained by Fourier transformation of the acquired data using a sine-bell apodization window and zero-filling up to 1024 points in both directions to reduce Gibbs ringing artifacts and interpolate the acquired 64×64 pixel points [1,2]. The field-of-view (FoV) of the image is 26 mm in both directions, defining a nominal spatial resolution of 0.4×0.4 mm^2 (pixel size). Since each point along the phase encoding direction is obtained by averaging four scans, with a recycling delay $T_R = 70$ ms, the total time to acquire the image was about 18 s. The gray scale of the image is proportional to the density of hydrogen nuclei in the rubber compound. For the present case, a high density region can be appreciated by higher brightness in the image. No contrast variation across the image was observed from T_2 and T_1 weighted images, suggesting that the material composition of the rubber is fairly homogeneous. Fig. 2b shows a high-resolution cross-section of the same profile acquired by X-ray microtomography for reference.

An important quality control issue is to monitor the geometry of the object during extrusion to assure that the dimensions stay inside the required standards. As typical deviations tolerated during production are of the order of 10%, for the profile shown in Fig. 2, size variations of the order of 200 μm need to be detected. Considering that the required precision is better than the spatial resolution achievable by MRI – at least in limited experimental times –, the main question regarding the application of MRI for this particular test is what is the spatial accuracy that can be achieved to extract the inner and outer contours from an image with a given nominal pixel resolution? This is a problem known from others image processing areas, where numerical algorithms have been presented to find the position of sharp edges with a precision better than the pixel size [8–10].

3.1. Sub-pixel analysis

A simple algorithm to determine the interface position of an object is based on searching for the spatial point where the signal value decreases to half of the maximum amplitude in the image [10]. A key issue to implement this algorithm requires a previous interpolation of the real pixels defining the nominal resolution in the image, to considerably enhance the digital resolution. To show how the algorithm works as a function of the nominal resolution for the case of MRI, spin-echo imaging experiments were simulated varying the number of pixels N across a 2 mm thick sheet sample (Fig. 3a). For sufficient resolution (16 pixels covering the sample thickness), the square profile is very well reproduced by the MRI experiment, but when the number of pixels in the profile is reduced, its square shape starts to blur. Although poorer resolution leads to a more and more rounded shape, it is noticed that all curves pivot at the point of half-height amplitude, which is the position that corresponds to the edge of the sample. Unlike in the

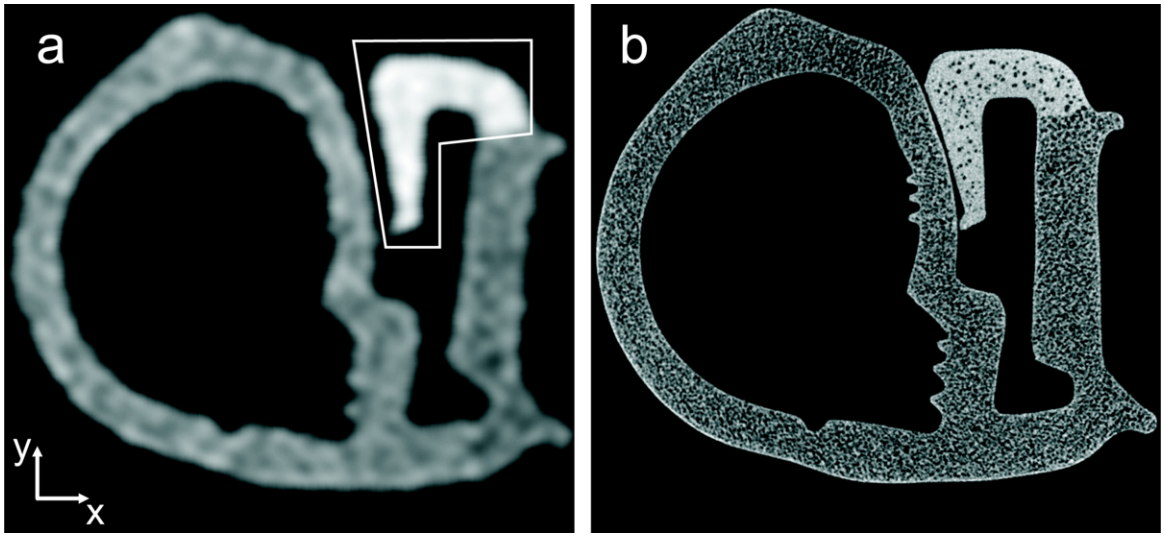

Fig. 2. (a) Slice selective 2D NMR image of a typical rubber fitting measured with a 0.5 T Halbach magnet. Four scans of a spin-echo sequence were averaged with an echo time $T_E = 0.8$ ms and repetition time $T_R = 70$ ms. The acquisition time was 18 s. The white frame indicates a region of higher foam density in the profile. (b) Two dimensional image of the same sample generated by an X-ray CT-scan (model: Skyscan 1172-70FOV, SkyScan N.V., Kontich, Belgium). From the gray-scale value, which is proportional to the absorption of X-ray radiation, one can discriminate the foam cells and the two sections with different densities. The spatial resolution in this image is 29.7 μm/pixel and the acquisition time was about 40 min.

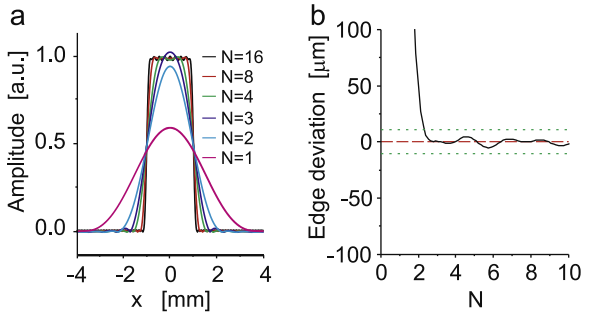

Fig. 3. (a) One dimensional amplitude profiles of a 2 mm thick flat sample obtained by simulating a spin-echo MRI experiment for different number N of pixels covering the thickness of the sample. Each profile is the Fourier transform of the echo signal apodized with a sine-bell window and zero-filled to 2^{12} points. (b) Deviation of the edge position measured with respect to the real edge location plotted as a function of the number N of pixels in the profile. An error lower than 10 μm is predicted for $N > 2.3$.

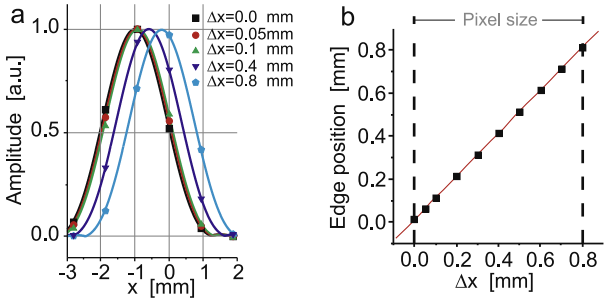

Fig. 4. (a) One dimensional amplitude profiles of a 2 mm thick flat sample displaced a distance Δx from the original central position located at $x_0 = -1$ mm. The curves were obtained by simulating a spin-echo MRI experiment for each different value of Δx. Solid lines represent a profile obtained after Fourier transforming the echo signal, previously apodized and zero-filled as described before. The filled symbols represent the same profiles obtained without the interpolation. (b) Position of the right interface of the sample obtained by taking the half-height value in the interpolated profile of (a), as a function of the displacement Δx. The perfect correlation between real and measured interface position demonstrate that the proposed methodology allows the determination of sharp edges with sub-pixel resolution.

case of digital processing where the interpolation is done directly in the final image, for the case of MRI the interpolation is achieved by zero-filling the time domain data previous to the Fourier transformation.

Although this numerical method provides considerable resolution enhancement, it leads to confident results only if the nominal resolution is better than a threshold value that depends on the sample structure. If the nominal resolution is poorer than a critical limit, the position of the interface, measured at half-height, shifts and does not provide the actual sample thickness anymore. Fig. 3b shows the difference between the interface position obtained by taking the half-height point and the real edge position as a function of the number N of pixels in the profile. The error stays below 10 μm if at least $N_{min} = 2.3$ non-interpolated pixels are inside the object. For example, for the case of the 2D image shown in Fig. 2a, which has a wall thickness of about 2 mm, a pixel size of 0.8 mm would be enough to determine the inner and outer interfaces with good accuracy. Provided that the number of pixels across the sample wall to be measured stays above this limit, this simple algorithm can quickly be applied to reconstruct the sample shape with enhanced spatial accuracy. It is important to notice that although the algorithm leads to accuracies to determine the edges more than one order of magnitude better than the nominal pixel size, by no means it would allow to resolve structures smaller than the pixel size.

One question that may arise is wether or not the position of the interface extracted from the algorithm shifts when the object interface is at different physical positions in between two real pixels. To answer this question we simulated spin-echo imaging experiments varying the position of the 2 mm thick sheet sample in steps smaller than the nominal resolution. To do this the nominal resolution was set to 0.8 mm, which is the lowest resolution that satisfies the required resolution limit explained above. The sample was initially centered at $x_0 = -1$ mm and the central position was moved in steps Δx lower than the pixel size covering a range of the order of one pixel. Fig. 4a shows the profiles corresponding to different displacements Δx. The continuous lines correspond to the profiles obtained after Fourier transforming the echo signal, previously window-filtered with a sine-bell function and zero-filled to 4096 points. On the other hand it is also shown with solid symbols, the corresponding profile data obtained without the interpolation procedure. It can be seen that the amplitude of a certain pixel point (solid symbol) varies depending on the displacement of the profile, but they always remain at the same spatial places. For each of the interpolated profiles the interface position was determined by searching for the half-height signal amplitude point in the profile. Fig. 4b shows the excellent agreement between the real position Δx (abscissa) and the measured one (ordinate), proving that the method determines edge positions with sub-pixel resolution.

In cases where the sample under study presents regions with different amplitudes, like the sample studied in this work, which combines foamy rubber with two different densities, the algorithm must be applied in sectors where a single maximum of signal can be defined. This can be achieved by dividing the image in two spatial regions (Fig. 2a). In case of more complex structures it could be possible to use information provided by other contrast parameters like T_2 or T_1 and to implement powerful MRI segmentation methods like the ones used in medical diagnostic imaging with satisfactory results even under the challenging conditions determined by biological tissues [17].

By applying the described algorithm to the image shown in Fig. 2a, it is possible to reconstruct the inner and outer contours of the object (Fig. 5). From this contour image it is possible to measure geometrical dimensions, like wall thickness at different positions, or the full size of the internal voids, which are of interest for the industry. Since the wall of the rubber fitting is about 2 mm

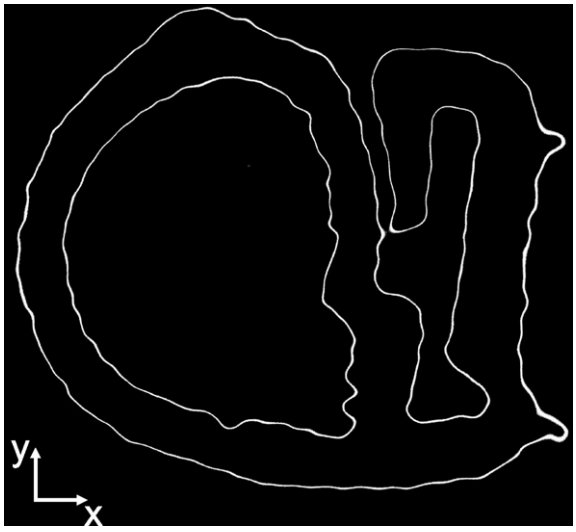

Fig. 5. Reconstruction of the rubber profile contour by identifying the half-height amplitude in the image.

thick, setting the pixel size to the maximum dimension allowed by the criteria discussed above ($N \geqslant 2.3$ across the wall), the number of steps along the phase direction can be reduced to minimize the total experimental time. For this particular case 32×32 pixels can be used. Once the spatial resolution is set, the accuracy to determine the interfaces from the 2D image depends on the signal-to-noise ratio (SNR) of the NMR experiment. Fig. 6a shows magnified 1D cuts obtained from 50 different 2D images. Each of the 2D images was measured with two scans of a spin-echo sequence applied under the same experimental conditions and without moving the rubber sample. It can be seen that due to the noise, the x position of the half-height point of the different curves fluctuates around a mean value $x = 0$. The standard deviation of this fluctuation defines the experimental error σ of the interface location identified from the MRI measurement. As the SNR increases, for example by increasing the number of scans, the error in the edge determination becomes smaller. This is appreciated in Fig. 6b where the inverse proportionality of both quantities, $\sigma \simeq SNR^{-1}$, is highlighted by the log–log plot. By averaging two scans, the SNR of the image is 25 and a $\sigma = 65$ μm is obtained. This accuracy is more than one order of magnitude better than the nominal resolution of the image and is sufficient for in-line quality control of rubber profiles since it is also lower than the measurement tolerance specified by the DIN ISO 3302-1 [18].

3.2. In-line control by MRI

Although the procedure described above was implemented on samples at rest, the obtained results prove that the resolution and sensitivity of MR images acquired in relatively short experimental times are enough to reconstruct the geometry of extruded rubber profiles with a precision better than the one required for quality control. In the present section the possible limiting factors affecting the methodology at the time of applying it to moving samples are discussed. Fig. 1a shows the potential places, in an extrusion line, where the MRI sensor can be mounted. The structure of the rubber to be monitored lies in a perpendicular plane (xy-plane) to the direction z of movement (see Fig. 1b). In conventional rubber extrusion processes velocity v values range from 0.1 m/s to 0.5 m/s, depending on the application [16]. For the present analysis an average velocity value of 0.3 m/s is assumed as a typical value.

The spin-echo sequence used to obtain the 2D images of the rubber profile measures the k-space line-by-line requiring a waiting time T_R between acquisitions. During T_R the sample moves and the different lines of the k-space are measured from different slices of the moving rubber resulting in a cross-sectional image averaged over a certain length along the sample. The length of the sample used to reconstruct the complete 2D image depends on the slice thickness, velocity v of the extrudates and on the total acquisition time. The latter is proportional to the number of pixels along the phase encoding direction, the number of scans, and T_R in between scans. For samples at rest in the magnet, the waiting time is about $3T_1$. But for in-line applications, the movement of the rubber refreshes the measured slice and depending on the velocity it can allow more frequent acquisitions. For a velocity of 0.3 m/s and a slice thickness of 10 mm, the refreshing would take 30 ms, while assuming a typical T_1 value of 100 ms for samples at 100 °C, a time of 300 ms would be needed to get the slice fully polarized again. In these conditions, after one scan is completed, the measured slice moves out of the sensitive region and the next magnetized slice is ready to be excited and detected in a time much shorter than $3T_1$. Then, the delay between experiments can be minimized. For images measured with 32 phase-encoding steps and two scans, the segmented k-space acquisition averages the shape of the moving rubber sample along 640 mm, and would take a time of about 2 s to be completed. This distance is, in general, much shorter than the length-scale of defects which can be of the order of several meters [11,12,16].

A remaining question to be answered is whether or not the continuous movement of the sample prevents it from getting polarized before reaching the measuring point (center of the magnet), and what is the influence of the movement in the excitation and detection of the signal. Considering that the T_1 of rubber formulations are of the order of 100 ms, and that the sample needs $3T_1$ to reach the equilibrium polarization value, at an average velocity of 0.3 m/s the sample would travel 0.1 m to get polarized. Since this distance is smaller than half of the magnet length l_M (see Fig. 1b), the sample is polarized when it reaches the center of the magnet. Excitation and detection are not instantaneous processes. Regarding excitation, pulse lengths of the order of 100 μs are needed to excite a 10 mm thick slice. If the sample travels at 0.3 m/s it would only move 30 μm during the excitation, which is a negligible distance in comparison with the thickness of the slice. Finally, since for the present case the detection process takes 640 μs the sample would move about 200 μm, which is also very small compared to the length of the rf coil l_c. It should be noted that, as the magnetic field gradients are applied perpendicular to the displacement direction it is possible to encode the spatial information of the running object without introducing geometrical distortions in the images. The previous analysis says that at speeds typically found in production sites in-line MRI measurements could be carried out without requiring additional cares like pre-polarization stages or particular excitation/detection schemes. However, as the cross-section measured with this method is an average over a certain length of the rubber, vibrations of the sample perpendicular to the movement direction can be problematic and must be avoided during the measurement process. A possible way of reducing them is by applying brushes also used for cleaning the surface of the profile as well as additional rollers.

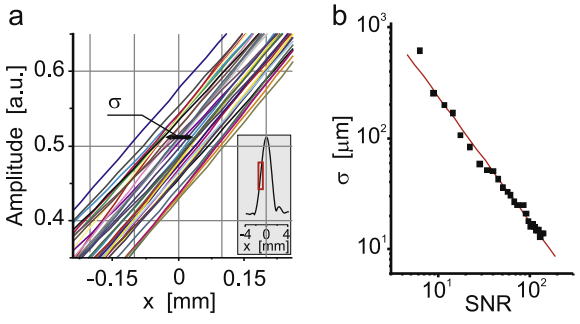

Fig. 6. (a) Magnification of the half-height region of 50 1D profiles of a rubber sample measured with the described MRI system. This series of experiments shows that the measurement uncertainty of the edge location is $\sigma = 65$ μm. Each image with 32×32 pixels and a resolution of 0.8 times 0.8 mm^2 in the plane was acquired in 5 s. (b) Dependence of the edge uncertainty, σ, on the SNR. A clear SNR^{-1} dependence can be appreciated in the plot.

4. Experimental

The magnet array used for this work is based on a recently proposed compact magnet geometry optimized for high-resolution NMR spectroscopy [5]. It is a modified Halbach configuration [19], where each ring is composed of fixed trapezoidal elements leaving parallel gaps between them to guide the movement of rectangular magnet blocks. These rectangular blocks can be moved radially in and out to mechanically shim the magnetic field in a highly efficient and accurate way [5], tackling the important source of inhomogeneity introduced by errors in the polarization of the magnet pieces. As the number of terms that can be generated to

shim the field scales with the number of movable pieces, the rings forming the present magnet included 12 rectangular blocks interleaved with 12 trapezoids. Moreover, to reduce field distortions along the cylinder axis due to the finite magnet length, this array was made from a stack of nine Halbach rings with their geometric proportions individually optimized. The total weight of the magnet including housing is around 100 kg. The final array is a cylinder 320 mm long with outer and inner diameters of 330 mm and 100 mm, respectively. Made from SmCo blocks the array generates a field of about 0.5 T, which corresponds to a resonance frequency of about 20 MHz for hydrogen nuclei. The homogeneity achieved applying the shimming process described in [5] to this scaled-up version of the magnet is better than 1 ppm in a spherical volume (DSV) of 40 mm diameter. The magnet was equipped with a solenoidal rf coil, 40 mm in diameter and 70 mm long made of a 6-turn copper stripe with winding widths optimized to excite and detect the NMR signal with high uniformity. The duration of a hard 90° pulse for this coil is 37 μs using an rf power of 80 W. Furthermore, the magnet is fitted with a three-axes actively shielded gradient coil system designed to minimize the generation of eddy currents. The coils have an efficiency of 0.015 T A^{-1} m^{-1} along the transverse directions and 0.006 T A^{-1} m^{-1} along the axis of the magnet, and can be switched in ramp times of 20 μs. They were driven by two double channel Tecron LVC 5050 gradient amplifiers supplying a maximum output current of 20 A per channel. The switching time was measured from the current monitor of the amplifiers as the time interval required for the current to rise from 10% to 90% of maximum value during the gradient pulse. All the experiments were performed using a Kea2 spectrometer produced by Magritek, New Zeland. It is a fully digital spectrometer with shaped rf pulse capability, which weighs less than 5 kg having a volume of $36 \times 23 \times 15$ cm^3.

5. Conclusions

In this work we demonstrated that by applying a simple edge-detection algorithm to low-resolution MR images it is possible to determine non-invasively the internal and external geometry of rubber profiles with a spatial accuracy one order of magnitude better than the nominal pixel size. The resolution and sensitivity of the images required for the algorithm to provide a defined spatial accuracy were explored in order to determine the minimum experimental time. The obtained results prove that images acquired with a mobile MRI system in experimental times acceptable for the discussed application can be used to reconstruct the geometry of extruded rubber profiles with micrometer precision, which is better than the one required for quality control. This shows that mobile MRI is at the stage to be applied for in-line monitoring of extruded products.

Acknowledgment

This project was supported by the Deutsche Forschungsgemeinschaft Grant CA660/3-1.

References

[1] B. Blümich, NMR Imaging of Materials, Clarendon Press, Oxford, 2000.
[2] P.T. Callaghan, Principles of Nuclear Magnetic Resonance Microscopy, Clarendon Press, Oxford, 1991.
[3] J. Perlo, F. Casanova, B. Blümich, Ex situ NMR in highly homogeneous fields: H-1 spectroscopy, Science 315 (2007) 1110–1112.
[4] E. Danieli, J. Mauler, J. Perlo, B. Blümich, F. Casanova, Mobile sensor for high resolution NMR spectroscopy and imaging, J. Magn. Reson. 198 (2009) 80–87.
[5] E. Danieli, J. Perlo, B. Blümich, F. Casanova, Small magnets for portable NMR spectrometers, Angew. Chem., Int. Ed. 49 (2010) 4133–4135.
[6] P.J. McDonald, The use of nuclear magnetic resonance for on line process control and quality assurance, in: A.G. Gaonkar (Ed.), Food Processing: Recent Development, Elsevier, Amsterdam, 1995, pp. 23–36.
[7] B.P. Hills, K.M. Wright, Motional relativity and industrial NMR sensors, J. Magn. Reson. 178 (2006) 193–205.
[8] D. Marr, E. Hildreth, Theory of edge-detection, Proc. R. Soc. London, B 207 (1980) 187–217.
[9] J. Canny, A computational approach to edge-detection, IEEE Trans. Pattern Anal. Machine Intell. 8 (1986) 679–698.
[10] C. Demant, B. Streicher-Abel, P. Waszkewitz, Industrial Image Processing – Visual Quality Control in Manufacturing, Springer-Verlag, Berlin, 1999.
[11] J.L. White, Rubber Processing: Technology, Materials, Principles, Hanser Publishers, Munich, Vienna, New York, 1995.
[12] C. Rauwendaal, Polymer Extrusion, fourth ed., Hanser Gardner Publications, Munich, Vienna, New York, 2001.
[13] R. Brown, Physical Testing of Rubber, fourth ed., Springer Science and Business, New York Media, 2006.
[14] U. Masberg, Die Bedeutung der Freigabekritierien fr die Weiterverarbeitung, Kautsch. Gummi Kunstst. (KG) 60 (2007) 394–397.
[15] C. Liguori, A. Paolillo, A. Pietrosanto, An on-line stereo-vision system for dimensional measurements of rubber extrusions, Measurement 35 (2004) 221–231.
[16] W. Michaeli, U. Dombrowski, U. Husgen, Extrusion Dies for Plastics and Rubber: Design and Engineering Computations, third ed., Hanser Gardner Publications, Munich, 2003.
[17] L.P. Clarke, R.P. Velthuizen, M.A. Camacho, J.J. Heine, M. Vaidyanathan, L.O. Hall, R.W. Thatcher, M.L. Silbiger, MRI segmentation – methods and applications, Magn. Reson. Imag. 13 (1995) 343–368.
[18] http://www.ralicks.de/deutsch/toleranzen.htm.
[19] K. Halbach, Design of permanent multipole magnets with oriented rare-earth cobalt material, Nucl. Instrum. Methods 169 (1980) 1–10.